Mon. Not. R. Astron. Soc. **289**, 831–846 (1997)

Optical, infrared and millimetre-wave properties of Vega-like systems – III. Models with thermally spiking grains

R. J. Sylvester,[1] C. J. Skinner[2] and M. J. Barlow[1]

[1]*Department of Physics & Astronomy, University College London, Gower Street, London WC1E 6BT*

[2]*Space Telescope Science Institute, 3700 San Martin Drive, Baltimore, MD21218, USA*

Accepted 1997 March 27. Received 1997 March 20; in original form 1996 December 12

ABSTRACT

Vega-like stars are main-sequence stars that exhibit excess IR emission due to circumstellar dust grains which are probably distributed in discs. We have recently published an observational data base for a large sample of candidate Vega-like systems, comprising optical, near-IR and mm/submm-wave photometry, and mid-IR spectra. In a previous paper we presented radiative transfer models of eight sources from our sample that had low fractional excess luminosities. Here we present models of a further eight sources, all with large fractional excess luminosities dominated by excess emission at near-IR wavelengths. It was found that no single distribution of dust grains at thermal equilibrium in a disc could simultaneously match the excess emission at near-IR and longer wavelengths. We attempted to model the near-IR emission as due to thermally spiking small grains, which can temporarily attain the high temperatures required to produce excess near-IR emission. A near-IR spectrum of SAO 186777 shows the 3.3-μm UIR emission band, confirming our earlier detection of UIR emission at longer wavelengths, and suggesting that small carbonaceous particles are responsible for some of the near-IR emission. The thermally spiking models were only partially successful and many of the sources required the presence of grains emitting in thermal equilibrium at ~ 1000–1500 K. These grains must either be located very close to the stars (<1 au), or else be powered by accretion luminosity.

Calculations of the optical depths of the model discs suggest the discs are optically thick at visual wavelengths; optically thick modelling of these sources is desirable. The discs are optically thin at mm wavelengths, allowing us to confirm the presence of large grains in the discs. The stars presented in this paper may well be younger than the prototype Vega-like stars.

Key words: circumstellar matter – planetary systems – infrared: stars.

1 INTRODUCTION

Vega-excess, or Vega-like, systems are main-sequence stars that display substantial far-IR excess emission. The best known Vega-excess stars are α Lyr itself and β Pic. The excess emission is ascribed to circumstellar dust grains orbiting in a disc or ring structure (see e.g. Aumann et al. 1984).

A number of searches of the *IRAS* catalogues have found other candidate Vega-like stars (e.g. Aumann 1985; Walker & Wolstencroft 1988). Comprehensive reviews of the Vega-excess phenomenon and its relation to the formation of extra-solar planets can be found in Backman & Paresce (1993) and Ferlet & Vidal-Madjar (1994).

We have recently published the results of a major observational survey of a sample of some 24 Vega-like stars, including *UBVRI* optical photometry, near-IR photometry, mid-IR spectroscopy and mm/submm-wave photometry (Sylvester et al. 1996, henceforth Paper I). We presented models of a subset of our sample (Sylvester & Skinner 1996, henceforth Paper II), comprising the stars with no detectable near-IR (1–5 μm) excess emission. The models were produced using a radiative transfer code based on that used by Skinner, Barlow & Justtanont (1992) to model SAO 179815 (HD 98800) and similar to that used by Skinner et al. (1995) to model SAO 26804. In this paper, we present models of a another subset of stars from Paper I. These stars are distinguished by their excess emission at near-IR wavelengths, and the large fractional excess luminosity of the dust. Most of them show Hα emission and other spectroscopic evidence of youth (Dunkin, Barlow & Ryan 1997b); they may be transition objects between the Herbig Ae/Be or T Tauri phases and established main-sequence stars (Waelkens, Bogaert & Waters 1994; Dunkin et al. 1997b).

2 THERMAL EQUILIBRIUM MODELLING

The modelling code described in Paper II, to which the reader is referred for details, was used to model all the stars in this paper. Briefly, it uses optically thin radiative transfer methods to calculate the temperature of grains distributed in a disc around the star, which is itself modelled using a Kurucz (1991) model atmosphere. The spectral energy distribution of the emission from the star–disc system is then calculated. A wide range of grain sizes is used, with a power-law size distribution; the variation of dust density within the disc with distance from the star was also treated as a power law.

The central star was defined by its effective temperature, surface gravity and radius (all determined from the spectral type), and its distance (determined from optical photometry, adopting the absolute magnitude calibration of Schmidt-Kaler 1982). The dust grains were described by their composition, their maximum and minimum sizes ($a_{\rm min}$, $a_{\rm max}$), and the power-law index, γ, for the size distribution. For all the models, $a_{\rm min}$ was set to 50 Å.

The disc structure was described by its inner and outer radii ($R_{\rm in}$, $R_{\rm out}$), the density-distribution index, β, and the total mass of the disc, $M_{\rm disc}$. The dust temperature was calculated as a function of grain size, composition and distance from the central star, by applying the condition of radiative equilibrium.

Output from the model was produced in two forms: spectral energy distributions (SEDs), and simulated fluxes in the four *IRAS* bands and in two mm-wave bands for comparison with James Clerk Maxwell Telescope (JCMT) observations. For a detailed description of how the various model parameters affect the predicted SED, we refer the reader to Paper II.

3 MODELLING WITH SMALL GRAINS

As shown in Paper I, several Vega-excess stars display excess near-IR emission, e.g. SAO 77144 (HD 35187) and SAO 183986 (HD 143006). Inspection of the spectral energy distributions suggests that this excess is not merely the short-wavelength extension of the excess seen at mid- and far-IR wavelengths, but rather that there is a double-peaked structure to the overall excess energy distribution.

This may imply that there is more than one distinct spatial distribution of dust, and/or that there is more than one type of grain behaviour taking place. The first scenario, that there are two or more populations of grains in thermal equilibrium, runs into the problem that the dust temperatures required to produce a near-IR excess, approximately 1500 K, are higher than the sublimation temperature of circumstellar dust (approximately 1000 K). In other words, it would be impossible for dust to survive at the required temperatures for an extended period of time. Even if the evaporating dust was continuously being replenished, for instance by dust falling in from the cool outer regions of the disc, it may still be destroyed before reaching a temperature of 1500 K.

We therefore consider the second possibility – that there is another physical process at work to produce the observed near-IR excesses.

3.1 The small-grain hypothesis

Such a process was suggested by Greenberg (1968), who pointed out that the energy gained by a small grain upon absorption of a single photon could be comparable to the energy content of the grain. The grain would therefore not be in thermal equilibrium, but would undergo temperature fluctuations. Thermally spiking small grains were proposed by Sellgren, Werner & Dinerstein (1983) to explain observations of reflection nebulae which showed near-IR continuum and unidentified-infrared (UIR)-band emission. These small grains (radius ~10 Å) have a very low heat capacity, and so can be heated to temperatures of the order of 1000 K by the absorption of a single UV photon.

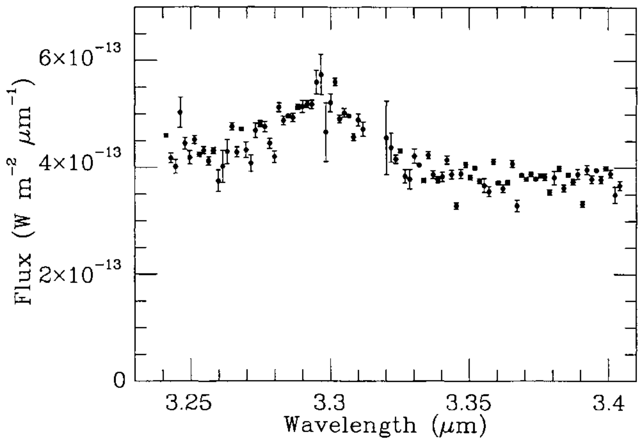

Figure 1. CGS4 spectrum of SAO 186777 (HD 169142). This spectrum clearly shows emission in the 3.3-μm UIR band. The spectrum was obtained for us in UKIRT Service time. The 75 line mm^{-1} grating was used with a 1.5 arcsec wide slit, aligned east–west to yield a spectral resolving power of 1000. The integration time was 160 s. The telescope secondary was chopped east–west with a 20-arcsec throw; BS 6378 was used as the standard star.

Small grains have been used to model the emission from the planetary nebula Abell 30, and gave a good fit to the near-IR observations (Borkowski et al. 1994). Hartmann, Kenyon & Calvet (1993) and Natta, Prusti & Krügel (1993a) suggested that small grains could be responsible for a significant fraction of the near-IR excess emission of Herbig Ae/Be stars.

Several of the Vega-like stars in our sample show mid-IR UIR-band emission (Paper I), which is thought to be due to small carbonaceous particles, such as polycyclic aromatic hydrocarbons (PAHs). This lends weight to the suggestion that thermally spiking grains are present in Vega-like discs. A 3-μm spectrum of SAO 186777 obtained with the CGS4 spectrometer as a UKIRT Service observation is presented in Fig. 1. The spectrum shows emission in the 3.3-μm UIR band, while only 25 per cent of the underlying continuum is due to the photospheric radiation field of the A5Ve star.

The 3.3- and 11.3-μm UIR bands are both thought to arise from the C–H bond in PAHs; this allows the temperature of the emitting material to be estimated from the band strengths (de Muizon, d'Hendecourt & Geballe 1987). We find an integrated flux of $(4.4 \pm 0.6)\times10^{-15}$ W m^{-2} in the 3.3-μm band and $(1.0 \pm 0.1)\times10^{-14}$ W m^{-2} in the 11.3-μm band (having scaled the CGS3 10-μm spectrum to the *IRAS* 12-μm flux – see Paper I).

This gives a flux ratio $I(11.3)/I(3.3) = 2.4$, which is similar to that found for the Red Rectangle (Léger & d'Hendecourt 1987). Using fig. 3 of de Muizon et al. (1987), this ratio gives a temperature of 1000±80 K. This is the average temperature of the PAH molecules as they cool after a thermal spike, and is roughly 2/3 of their peak temperature. Coulson & Walther (1995) performed similar calculations for SAO 206462, and deduced a temperature of 515±25 K. The higher temperature for SAO 186777 may be due to the 'harder' radiation field, as it has an earlier spectral type. From these results it is clear that there is a thermally spiking component of the dust around these Vega-excess stars, which reaches temperatures of at least several hundred K.

3.2 Calculating the temperature distribution

The thermal behaviour of a small grain in a radiation field can be described by its probability distribution function $P(T)$, where $P(T)\mathrm{d}T$ is the probability of finding the grain in the temperature interval $(T,\ T+\mathrm{d}T)$. To determine this function, the method of Guhathakurta & Draine (1989, henceforth GD89) was used, whereby the range of possible temperatures is divided into a number of discrete bins, and the probability of a grain occupying each bin is calculated.

For the present work, typically 300 bins were used: experimentation showed that this was sufficient to avoid any problems due to having too coarse a spacing, and gave results that showed negligible differences compared with those obtained using a much larger number of bins (several thousand). Using a small number of bins gives considerable savings in the amount of computer time required.

Following GD89, we treated the heating due to long-wavelength (λ >1 mm) radiation as continuous, rather than discrete photon interactions, to ensure non-zero minimum grain temperatures. Typical values of $T_{\rm min}$ were found to be $\sim$0.5 K.

The temperature for the highest enthalpy bin, $T_{\rm max}$, was usually set to 2000 K, as it was found that the probability of a grain being above this temperature was normally extremely small. Also, grains much hotter than 2000 K will lose energy by sublimation rather than by radiative cooling (GD89; Voit 1991) and so will not contribute significantly to the model emission.

If the grains are near thermal equilibrium (i.e. multiphoton absorption is important), grains at low temperatures make a negligible contribution to the emission, because the probability of a grain being at a low temperature is very small, and because cool grains emit very weakly. In order not to 'waste' enthalpy bins on these unimportant temperatures, a third temperature parameter, $T_{\rm base}$, was introduced such that the temperature interval $T_{\rm min} < T < T_{\rm base}$ is spanned by only 10 equally spaced enthalpy bins, allowing the bins in the range $T_{\rm base} < T < T_{\rm max}$ to be more closely spaced (equally spaced bins were also used in this regime).

To determine the probability distribution function of the grain, GD89 defined a set of probabilities, $P_k(t)$, as the probability of the grain being in the kth enthalpy bin at a time t. As its temperature fluctuates, a grain will move among the bins. An ensemble of identical small grains in a static radiation field will exist in a dynamical equilibrium where the number of grains in a particular bin remains constant with time, although each individual grain is making transitions among the bins as it absorbs photons and subsequently cools down. Steady-state probabilities, $P_k^{\rm SS}$, can therefore be defined.

The grain cooling process is treated as continuous – discrete cooling events, where a grain can go from one state to a cooler one without passing through all the intermediate states, are not allowed in the GD89 treatment. This greatly simplifies the problem of solving the equations to determine the steady-state probabilities. Siebenmorgen, Krügel & Mathis (1992) pointed out that for real grains, discrete cooling events could occur, and suggested that this would give rise to more far-IR and submm emission than predicted by the GD89 method.

For the extreme example given by Siebenmorgen et al. of a 5-Å grain 0.16 pc from a B1V star, allowing discrete cooling events increases the submm flux by a factor of approximately 20. However, for Vega-excess stars, such a discrepancy would make no appreciable difference to the total submm fluxes, since the equilibrium emission of 'normal' large grains is typically 2–3 orders of magnitude stronger than the small-grain emission at submm wavelengths.

GD89 also considered discrete heating due to collisions between the grain and other particles, but collisional heating was ignored for the present work.

3.3 Output

The results from the model were recorded in two forms – a probability distribution function (pdf) and a spectral energy distribution. The pdf was found by converting the discrete steady-state probabilities into values of the continuous function $P(T)$. This was achieved by dividing the probability of a grain being in a bin by the temperature interval covered by the bin, ΔT_i. The quotient obtained is a good approximation to the value of the pdf at the temperature T_i. Since a grain is required to be in one or other of the bins, the value of the pdf is zero for $T < T_{\rm min}$ and for $T > T_{\rm max}$. Tests using a model of a B3V star gave good agreement with the results of GD89.

The spectral energy distribution was determined by calculating the spectrum expected from a grain at the temperature of each bin, and then adding all N such contributions together, weighted by their respective probabilities:

$$S_{\lambda,\rm out} \propto Q_{\rm abs}(\lambda) \sum_{i=1}^{N} P_i^{\rm SS} B_\lambda(T_i), \tag{1}$$

where $B_\lambda(T)$ is the Planck function, and T_i is the temperature of the ith bin. The absorption (and hence emission) efficiency $Q_{\rm abs}$ and the probability distribution are functions of grain size, but for the present modelling, only a single size of small grain was used in any given model, rather than a size distribution.

4 SYSTEMS SELECTED FOR MODELLING

The Vega-like systems that we model in this paper are all taken from the sample that was presented in Paper I, and are distinguished by having substantial near-IR excess emission. In total, eight stars are modelled in this paper.

Table 1 lists the stars to be modelled in this paper, and summarizes their observational properties, as discussed in detail in Paper I. Listed are spectral type, V-band magnitude, and fractional excess luminosity, $L_{\rm IR}/L_\star$, which is the ratio of the luminosity of the dust disc to that of the central star. For most of the stars in the present paper, $L_{\rm IR}/L_\star$ is greater than 1/4, the maximum for a physically thin disc, implying that the discs must be substantially flared, or even accompanied by spherical envelopes. Accretion of matter through a disc can add extra IR luminosity; however, in the present models we only consider the reprocessing of starlight.

5 MODELLING PROCEDURE

The modelling technique treats the discs as being optically thin to the stellar radiation powering their emission: for the stars with the largest fractional luminosities, this is not likely to be true. Optically thin models do, however, provide a useful approximation to the circumstellar environments of Vega-excess stars, in the absence of more elaborate techniques.

The procedure for combining equilibrium and small-grain models for stars with near-IR excess emission was to use the equilibrium disc model first, and fit the mid-IR to mm-wave data.

Table 1. Observational properties and adopted stellar parameters of the present sample.

SAO	HD	Spectral Type	Ref.	V mag.	Ref.	$\frac{L_{\mathrm{IR}}}{L_\star}$	T_{eff}	log g	$R_\star$ $\mathrm{R}_\odot$	d pc
77144	35187	A2/3 IV/Ve	1	7.80	8	0.14	9000	4.0	2.1	202
131926	34282	A0	2	9.88	8	0.39	9500	4.0	2.7	547
183956	142666	A8Ve	3	8.65	8	0.34	7500	4.0	1.7	116
183986	143006	G5Ve	4	10.18	8	0.56	5750	4.5	0.8	82
184124	144432	A9/F0 Ve	5	8.17	8	0.48	7250	4.0	1.6	110
186777	169142	A5Ve	3	8.13	9	0.24	8250	4.0	1.9	145
206462	135344	F8Ve	6	8.63	6	0.64	6250	4.5	1.3	84
226057	139614	A7Ve	7	8.27	9	0.39	7750	4.0	1.8	151

References: (1) Zuckerman, Forveille & Kastner (1995); (2) Henry Draper Catalog; (3) Dunkin, Barlow & Ryan (1997a); (4) van der Veen et al. (1994); (5) Houk (1982); (6) Coulson & Walther (1995); (7) Houk (1978); (8) Paper I; (9) van der Veen, Habing & Geballe (1989).
An 'e' in the spectral type indicates that Hα has been observed in emission, usually by Dunkin et al. (1997b). The value of $L_{\mathrm{IR}}/L_\star$ for SAO 186777 was calculated adopting the Dunkin et al. spectral type, and differs from the value in Paper I.

All models that gave good agreement with the mid- and far-IR observations were found to make negligible contributions to the near-IR flux, which allowed the two modelling techniques to be used nearly independently.

Having obtained a well-fitting disc model, small-grain models were computed, with the grains situated at the inner radius found for the disc models. The required mass of small grains was determined by fitting the near-IR excess fluxes. The emission from the small grains was then simply added to the fluxes from the disc model, which included the photospheric contribution. Sometimes the non-zero flux from the small grains in the mid-IR caused the fit to the CGS3 spectrum to deteriorate; a slight increase in the inner radius of the disc model generally sufficed to decrease the disc model's contribution at 10 μm, and allowed the fit to be recovered.

The radii of the small grains were usually set to 3 or 5 Å. The smaller a grain is, the more likely it will be to undergo temperature spiking; these sizes were chosen to maximize the spiking, while retaining enough atoms in the grain for them plausibly to emit near-IR continuum radiation.

If it was found that thermally spiking small grains gave unsatisfactory fits to the near-IR excess, the distance between the small grains and the star was reduced until the emission from the grains (now approximately in thermal equilibrium) matched the near-IR excess spectral energy distribution. This provided useful measures of the grain temperature characterizing the near-IR excess, and lower limits on the amount of mass required to produce such an excess. The mass lower limits and dust temperatures are valid irrespective of the mechanism that is actually heating the grains – thermal spiking by excess UV photons, equilibrium heating of grains close to the star, or even some process intrinsic to the disc, such as collisional heating.

The disc outer radii were usually set to 10 arcsec, corresponding to the approximate size of the JCMT beam. If a larger value was used, only the flux arising in the inner 20 arcsec (diameter) was included for the tabulated values of the predicted mm-wave fluxes, to allow comparison with the JCMT measurements.

The equilibrium models are labelled with a letter followed by two numbers. The letter refers to the type of dust material used: M for astronomical silicate, C for amorphous carbon (AC), and B for a blend of silicate and carbon. The two numbers refer to γ, the index of the power-law grain size distribution $N(a) \propto a^{-\gamma}$, and β, the power-law index for the density distribution, $n(R) \propto R^{-\beta+1}\mathrm{d}R$ (see Paper II for details). Decimal points and minus signs are symbolized with p and m respectively. Suffixes a, b, etc. could be used to distinguish between models with the same values of γ and β.

6 RESULTS

6.1 SAO 77144 (HD 35187)

SAO 77144 is listed in the *Hipparcos* Input Catalogue (Turon et al. 1992) as a double star. The two components are separated by 1.2 arcsec, and have equal V magnitudes. For the purposes of modelling this system, it was assumed that the two component stars were identical, but that the grains were heated by only one of them. The results of modelling SAO 77144 are summarized in Table 2.

A grid of pure silicate models was produced (models M22–M2p50p7). Values of inner radius and disc mass were chosen to obtain a good fit at 25 and 60 μm. As can be seen in Paper I, there is some discrepancy between the *IRAS* 12-μm flux and the CGS3 spectrum of this source. Modelling using a 5.5-arcsec aperture showed that the discrepancy was not due to beam size effects. We assume that the absolute flux calibration of the CGS3 spectrum was in error; the CGS3 spectrum plotted in Fig. 2 has been scaled up by 1.45 to make it consistent with the *IRAS* 12-μm flux.

A number of equilibrium grain models were run using a blend of 75 per cent silicate grains and 25 per cent amorphous carbon grains (models B22–B31). Table 2 summarizes the fit of these models to the 12 μm to 1.1 mm spectrum of SAO 77144. Model M2p50p7 gives a good fit to the observations, and is plotted in Fig. 2.

The near-IR excess emission of SAO 77144 was modelled using the small-grain code. Small (3-Å radius) silicate grains at 3.3 au from the star were found to be out of thermal equilibrium, and gave a good fit to the near-IR excess photometry. However, they produced a strong silicate emission feature, far in excess of the observed silicate feature in the CGS3 spectrum.

3 Å radius grains of AC gave a good fit to the near-IR photometry without giving rise to spectral features. Combining the two materials, it was found that silicates could form up to approximately 10 per cent of the small-grain population before giving rise to too strong a silicate feature. A mass of $1.2 \times 10^{-5} M_{\mathrm{Earth}}$ of small AC grains at 3.3 au was needed to provide the observed amount of near-IR flux.

Grains of radius 3 Å (the largest that show significant departures from thermal equilibrium) contain approximately 30 atoms, which

Table 2. Models for SAO 77144 (HD 35187).

Model	γ	β	R_{in} au	R_{out} au	M_{disc} $M_\odot$	a_{max} μm	F_{12}	F_{25} Jy	F_{60}	F_{100}	$F_{0.8}$	$F_{1.1}$ mJy
Observations							5.4	11.5	8.0	5.0	115	80
(± error)							0.3	0.7	0.8	0.5	22	10
M22	2	2	8.7	1430	9.2×10^{-6}	1000	3.6	11.5	8.0	3.8	94	41
M21	2	1	4.0	1430	1.0×10^{-4}	1000	5.7	11.4	8.0	4.9	277	127
M12	1	2	7.4	1430	2.8×10^{-5}	1000	3.7	11.4	8.0	4.0	149	74
M11	1	1	2.5	1430	2.6×10^{-4}	1000	7.0	11.4	8.0	5.1	452	239
M31	3	1	41.4	1430	4.0×10^{-6}	1000	1.4	11.5	8.0	3.9	39	14
M2p51	2.5	1	16.0	1430	2.2×10^{-5}	1000	3.5	11.4	8.0	4.4	119	48
M30p5	3	0.5	16.7	1430	6.2×10^{-6}	1000	2.9	11.4	8.1	4.4	53	19
M20p5	2	0.5	0.3	1430	3.2×10^{-4}	1000	10.3	10.4	8.3	6.7	724	344
M2p50p5	2.5	0.5	4.0	1430	5.4×10^{-5}	1000	6.5	11.5	8.1	5.3	221	91
M2p50p7	2.5	0.7	8.7	1430	3.8×10^{-5}	1000	4.4	11.5	8.0	4.9	173	71
B22	2	2	10.7	1430	6.4×10^{-6}	1000	3.7	11.4	8.0	3.8	92	40
B21	2	1	4.7	1430	4.8×10^{-5}	1000	5.8	11.5	8.0	4.7	246	112
B31	3	1	51.5	1430	1.7×10^{-6}	1000	3.1	11.4	8.0	3.7	33	12

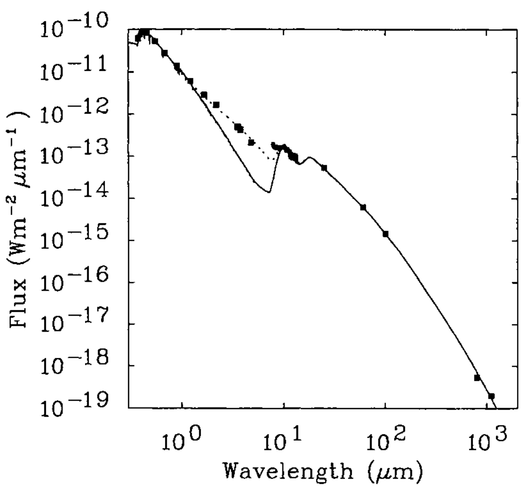

Figure 2. Results of modelling SAO 77144 (HD 35187). Filled squares: observed fluxes; solid line: model M2p50p7; dotted line: effect of adding small thermally spiking AC grains to M2p50p7.

is rather few for a realistic grain. For larger grains to be excited sufficiently to give rise to the observed near-IR excess emission, the stellar radiation field would need to be 'harder', i.e. have a greater UV component. Fig. 2 includes the emission from small grains. The details of the models in the 10-μm region are presented in Fig. 3.

Even after including the small-grain contribution, there is noticeable residual emission in the 8–9 μm part of the normalized CGS3 spectrum. This could well be due to the 7.7-μm UIR band, seen in the 10-μm spectra of a number of other Vega-excess stars (Paper I).

6.2 SAO 131926 (HD 34282)

This star has no MK spectral type, so the HD classification of A0 has been adopted, with luminosity class V assumed. No CGS3 spectrum is available for this source.

The near-IR photometry of SAO 131926 (Paper I) shows strong excess emission, so there is probably a contribution to the flux in the *IRAS* 12-μm band from the material responsible for the short-wave excess. Thus no attempt was made to fit the 12-μm point; the inner radius and disc mass were adjusted to give fits at 25 and 60 μm.

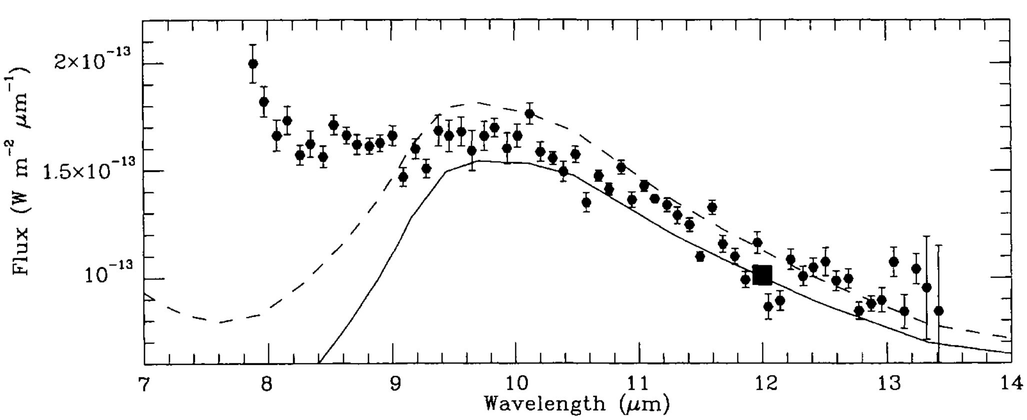

Figure 3. Detail of the SAO 77144 models in the mid-IR. Error bars: CGS3 spectrum scaled up by a factor of 1.45; large square: *IRAS* point; solid line: model M2p50p7; dashed line: effect of adding small grains.

Table 3. Models for SAO 131926 (HD 34282).

Model	γ	β	R_{in} au	R_{out} au	M_{disc} $M_\odot$	a_{max} μm	F_{12}	F_{25}	F_{60}	F_{100}	$F_{0.8}$	$F_{1.1}$
							Jy				mJy	
Observations							0.70	1.63	10.8	10.7	409	183
(± error)							0.07	0.10	0.1	0.1	27	17
M24	2	4	270	5470	3.3×10^{-3}	1000	0.03	1.67	10.8	17.6	>1Jy	828
M32	3	2	670	5470	1.8×10^{-4}	1000	0.01	1.83	10.9	9.2	155	56
M31	3	1	600	5470	3.2×10^{-4}	1000	0.01	1.65	11.0	10.7	230	84
M2p52	2.5	2	540	5470	2.3×10^{-3}	1000	0.01	1.76	10.8	11.6	897	383
M2p72	2.7	2	640	5470	8.4×10^{-4}	1000	0.01	1.67	10.8	10.5	413	165
M2p71	2.7	1	540	5470	1.4×10^{-3}	1000	0.01	1.63	10.8	11.5	565	230
M2p81	2.8	1	540	5470	7.8×10^{-4}	1000	0.01	1.74	10.7	10.8	375	146
B22	2	2	270	5470	9.4×10^{-3}	1000	0.08	1.68	10.8	15.7	>1Jy	>1Jy
B32	3	2	1200	5470	2.8×10^{-4}	1000	0.03	1.70	10.8	10.8	200	73
B2p72	2.7	2	1000	5470	1.3×10^{-3}	1000	0.03	1.82	10.7	11.5	464	185
C21	2	1	290	5470	2.5×10^{-2}	1000	0.12	1.58	10.6	12.1	303	111
C20p5	2	0.5	220	5470	4.3×10^{-2}	1000	0.14	1.76	10.8	13.4	458	170
C11	1	1	170	5470	7.4×10^{-2}	1000	0.02	1.65	10.9	10.2	215	78
C0p50p5	0.5	0.5	130	5470	1.9×10^{-1}	1000	0.03	1.67	10.8	12.2	394	146
C10p5	1	0.5	130	5470	1.6×10^{-1}	1000	0.03	1.67	10.8	12.2	395	146

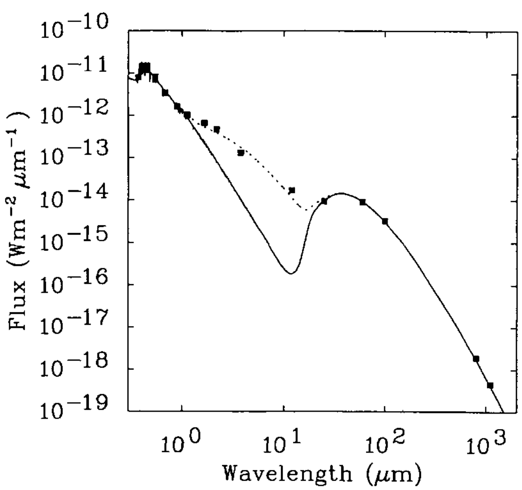

Figure 4. Results of modelling SAO 131926 (HD 34282). Solid line: model M2p72; dotted line: effect of adding small (3-Å radius) thermally spiking AC grains to model M2p72.

Grids of models were run using silicate grains (models M24–M2p81), silicate–AC blend (models B22–B2p72) and AC grains (C21–C10p5). Results are presented in Table 3. The best-fitting model was M2p72, the spectral energy distribution (SED) of which is presented in Fig. 4.

The near-IR excess of SAO 131926 was modelled using the small-grain technique. 3 Å radius grains (silicate or AC) were again found to be thermally spiking, and emitting in the near-IR. The fit is not ideal, with a *K*/*L*-band flux ratio that is too low. Using larger grains caused the fit to deteriorate. In the absence of a CGS3 spectrum, it cannot be determined whether the material is silicaceous or carbonaceous. With the 3 Å radius AC grains situated 530 au from the star, comparable to the inner radii of the disc models, it was found that approximately 1 Earth mass (M_{Earth}) of small grains was required to produce sufficient near-IR flux. This mass is roughly one per cent of the mass of grains in the disc model M2p72. The effect of combining this small-grain model with model M2p72 is illustrated in Fig. 4.

6.3 SAO 183956 (HD 142666)

Van der Veen et al. (1994) detected continuum emission from the A8Ve star SAO 183956 at 0.45, 0.8 and 1.1 mm, and found that the near-IR to mm-wave excess energy distribution could not be successfully modelled with a single dust shell.

The *IRAS* 12-μm point and the CGS3 10-μm spectrum from Paper I were treated as upper limits for the flux from the thermal equilibrium models, because the material responsible for the near-IR excess could make some contribution to the flux in the 10-μm region.

A grid of silicate models (models M21–M1p51p5: see Table 4) was produced, and one of grain blend models (B31–B11p1). The grid of silicate models shows that well-fitting models lie in a well-defined locus in (γ, β) space. Part of the 10-μm silicate feature may be due to small-grain emission, so it is not possible to use the contrast of the silicate feature to determine the value of the power-law size index γ, which would allow a unique model to be specified. Future high-resolution imaging of the system might allow the spatial distribution of the dust, and hence β, to be determined with sufficient precision to specify a unique model.

Small-grain models were produced for silicate and AC grains of radius 5 Å, situated 1.5 au from the star (roughly the inner radius of the disc models). These grains were found to be close to thermal equilibrium, with peak temperatures of around 400 K for silicate and 750 K for AC grains.

Grains of radius 3 Å exhibited thermal spiking behaviour, but the resulting spectral energy distribution of the small-grain emission peaked at too long a wavelength to give a good fit to the near-IR excess. A 3 Å radius grain contains only a few dozen atoms; any smaller 'grain' would be unlikely to emit the continuum near-IR radiation that is observed. For small-grain emission to be the dominant mechanism causing the near-IR excess, the radiation field of SAO 183956 must therefore be harder than that of the model atmosphere, i.e. excess ultraviolet emission would be required.

Some information can be deduced about the temperature and mass of the material that is responsible for the near-IR excess. This can be achieved by considering grains close enough to the star that they are hot enough to emit strongly in the near-IR.

Table 4. Models for SAO 183956 (HD 142666).

Model	γ	β	R_{in} au	R_{out} au	M_{disc} $M_\odot$	a_{max} μm	F_{12}	F_{25} Jy	F_{60}	F_{100}	$F_{0.8}$ mJy	$F_{1.1}$
Observations							8.7	11.5	7.5	5.1	351	167
($\pm$ error)							0.5	0.7	0.8	0.3	23	17
M21	2	1	1.8	1160	3.4×10^{-5}	1000	6.5	11.5	7.5	4.4	280	130
M20p8	2	0.8	1.1	1160	4.4×10^{-5}	1000	8.3	11.5	7.7	5.0	438	208
M20p9	2	0.9	1.4	1160	4.6×10^{-5}	1000	7.4	11.4	7.5	4.6	340	160
M20p9a	2	0.9	1.4	1160	5.4×10^{-5}	1000	3.6	9.0	7.6	5.0	395	186
M11	1	1	1.1	1160	1.1×10^{-4}	1000	8.2	11.6	7.5	4.7	463	248
M12	1	2	3.7	1160	8.5×10^{-6}	1000	4.0	11.4	7.6	3.7	137	68
M11p3	1	1.3	2.7	1160	5.0×10^{-5}	1000	4.2	10.2	7.5	4.4	291	152
M11p2	1	1.2	2.7	1160	7.0×10^{-5}	1000	3.8	9.6	7.5	4.6	355	187
M1p51	1.5	1	1.2	1160	7.7×10^{-5}	1000	7.7	11.4	7.5	4.7	417	213
M1p51p5	1.5	1.5	2.5	1160	2.5×10^{-5}	1000	5.2	11.5	7.5	4.0	180	87
B31	3	1	18.0	1160	1.6×10^{-6}	1000	3.9	11.4	7.4	3.6	38	14
B21	2	1	2.4	1160	4.2×10^{-5}	1000	6.0	11.4	7.6	4.4	260	120
B20p9	2	0.9	1.7	1160	5.4×10^{-5}	1000	7.5	11.6	7.5	4.5	304	142
B20p8	2	0.8	2.0	1160	7.8×10^{-5}	1000	5.3	9.9	7.5	4.9	401	189
B11	1	1	1.7	1160	1.4×10^{-4}	1000	7.8	11.7	7.5	4.6	431	231
B11p5	1	1.5	3.3	1160	3.5×10^{-5}	1000	4.7	11.3	7.5	4.0	200	103
B11p1	1	1.1	2.0	1160	1.1×10^{-4}	1000	6.3	11.2	7.5	4.4	360	191

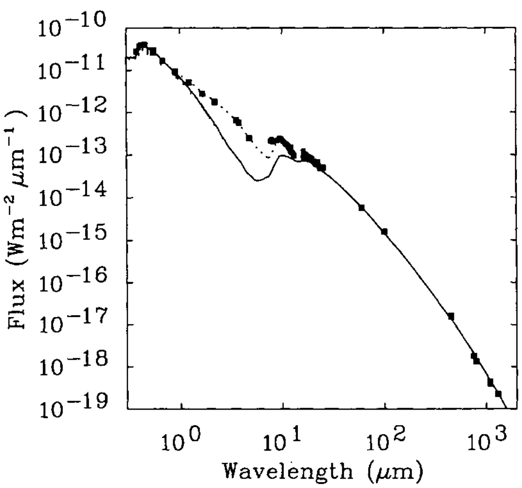

Figure 5. Results of modelling SAO 183956 (HD 142666). Solid line: model M20p9a; dotted line: effect of adding small (5-Å radius) silicate and AC grains in thermal equilibrium ($T\approx 1500$ K) to model M20p9a.

For SAO 183956, a fit to the observed near-IR excess could be obtained using 5-Å grains of silicate, close to thermal equilibrium, situated 0.2 au from the star. The temperature of such grains was ~1300 K, and a mass of $5\times10^{-7}M_{\rm Earth}$ was required to produce sufficient near-IR flux. For amorphous carbon grains, a distance of 0.4 au gave a good fit, with a temperature of 1300 K and a mass of $1\times10^{-6}M_{\rm Earth}$. These estimates are likely to be lower limits on the actual mass involved.

Using only small silicate grains gave too much contrast in the 10-μm silicate feature, implying that the near-IR excess is not due to only small silicate grains. Larger grains, with weaker 10-μm features, or grains of a different composition, must also be present. Adding the emission from small grains of AC to that of the silicate grains, in a 2:1 ratio, gives a silicate feature of similar strength to that observed. Combining the emission from this small-grain mixture with model M20p9a gives a good fit to the observed SED of SAO 183956 (Fig. 5). Details of the fit to the mid-IR spectrum of SAO 183956 are presented in Fig. 6.

No combination of models matched the 8–9 μm slope of the CGS3 spectrum. This wavelength region includes the wing of the

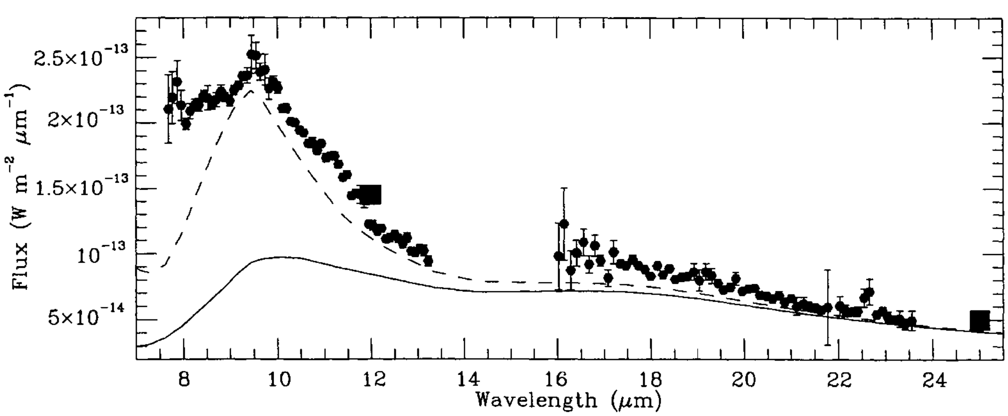

Figure 6. Detail of the SAO 183956 models in the mid-IR. Error bars: CGS3 spectrum; large squares: *IRAS* points; solid line: model M20p9a; dashed line: effect of adding small grains.

Table 5. Models for SAO 183986 (HD 143006).

Model	γ	β	R_{in} au	R_{out} au	M_{disc} $\mathrm{M}_{\odot}$	a_{max} μm	F_{12}	F_{25} Jy	F_{60}	F_{100}	$F_{0.8}$	$F_{1.1}$ mJy
Observations							0.86	3.2	6.6	4.8	233	114
($\pm$ error)							0.05	0.2	0.7	0.5	25	14
M22	2	2	5.1	850	6.9×10^{-6}	1000	0.23	3.2	6.5	4.7	193	86
M21	2	1	3.7	850	8.5×10^{-5}	1000	0.29	3.2	6.6	5.6	670	333
M21p8	2	1.8	5.0	850	1.1×10^{-5}	1000	0.23	3.2	6.6	5.0	229	103
M12	1	2	3.9	850	1.7×10^{-5}	1000	0.20	3.2	6.6	4.7	267	136
M12p3	1	2.3	4.1	850	1.1×10^{-5}	1000	0.19	3.2	6.6	4.6	229	115
M31	3	1	14.7	850	4.6×10^{-6}	1000	0.08	3.2	6.5	4.9	119	44
M2p51	2.5	1	10.0	850	2.8×10^{-5}	1000	0.13	3.2	6.6	5.6	361	157
M2p71	2.7	1	12.7	850	1.3×10^{-5}	1000	0.10	3.2	6.6	5.3	222	90
B22	2	2	6.7	850	1.1×10^{-5}	1000	0.28	3.2	6.6	4.9	209	93
B21	2	1	4.7	850	1.1×10^{-4}	1000	0.34	3.2	6.6	5.6	630	312
B21p8	2	1.8	6.5	850	1.6×10^{-5}	1000	0.28	3.2	6.7	5.0	242	110
B12	1	2	4.8	850	2.5×10^{-5}	1000	0.24	3.1	6.4	4.6	269	138
B13	1	3	5.7	850	1.0×10^{-5}	1000	0.21	3.1	6.6	4.5	205	102
B12p5	1	2.5	5.2	850	1.3×10^{-5}	1000	0.23	3.2	6.6	4.6	224	113
B31	3	1	23.4	850	4.0×10^{-6}	1000	0.29	3.2	6.5	4.8	103	38
C22	2	2	13.4	850	3.2×10^{-5}	1000	0.23	3.1	6.6	3.6	30	11
C21	2	1	9.4	850	1.8×10^{-4}	1000	0.28	3.1	6.6	4.6	87	32
C11	1	1	8.0	850	7.5×10^{-4}	1000	0.17	3.2	6.6	4.5	84	31
C0p50p5	0.5	0.5	5.0	850	2.8×10^{-3}	1000	0.27	3.2	6.6	6.0	214	80

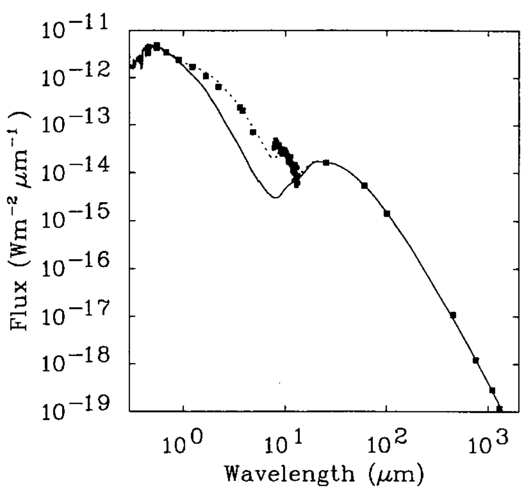

Figure 7. Results of modelling SAO 183986. Solid line: model B21p8; dotted line: effect of adding small thermal equilibrium silicate and AC grains ($T\approx1400$ K) to model B21p8.

strong 7.7-μm UIR band seen in the spectra of a number of Vega-excess stars (Paper I), and so it is possible that there is a UIR-band contribution to the 10-μm spectrum of SAO 183956. The inflection at approximately 11 μm in the observed spectrum (Fig. 6), not matched by the model spectrum, is also suggestive of a weak UIR feature.

6.4 SAO 183986 (HD 143006)

Van der Veen et al. (1994) suggested a spectral type for SAO 183986 of G5V, and made mm-wave continuum observations. As for SAO 183956, they found that it was impossible to obtain a satisfactory model fit to the observed excess energy distribution with a single dust shell.

A grid of models was run using astronomical silicate grains (models M22–M2p71: see Table 5). The presence of UIR-band emission in the 10-μm spectrum of SAO 183986 meant that a good fit could not be obtained to the shape of the spectrum. The spectrum was therefore treated as an upper limit to the model flux in that wavelength region. The inner radius and mass of the disc were adjusted to fit the *IRAS* data at 25 and 60 μm.

A second grid of models (B22–B31) was calculated, using a mixture of 75 per cent silicate and 25 per cent AC grains. One of the best-fitting blend models, B21p8, is presented in Fig. 7.

Using the small-grain code showed that 5-Å grains of silicate or AC located 4 au from the star (similar to the inner radii of the disc models) exhibited thermal spiking behaviour, but the resulting emission spectrum peaked at approximately 5 μm, giving a poor fit to the observed near-IR excess. Similar results were obtained using 3-Å grains. Good agreement with the observations could be obtained using 5-Å AC grains at 0.08 au from the star. These grains were close to thermal equilibrium, with a peak in the probability distribution function at approximately 1400 K. A mass of $4\times10^{-8}M_{\mathrm{Earth}}$ of these grains was required to provide sufficient near-IR flux.

A similar fit could be obtained using 5 Å radius silicate grains at 0.04 au from the star. These had a peak temperature of approximately 1500 K, and a mass of $1\times10^{-7}M_{\mathrm{Earth}}$ was required. However, these small silicate grains gave a strong silicate feature, exceeding the flux in the observed CGS3 spectrum. A superposition of these two small-grain models, with weighting factors of 0.8 for AC and 0.2 for silicate, gives a lower contrast silicate feature, which is in reasonable agreement with the 10–13 μm portion of the CGS3 spectrum. The effects of adding this model to model B21p8 are illustrated in Figs 7 and 8. The combined model gives a good fit to the general shape of the 9–13 μm emission, and clearly shows the presence of the 7.7- and 11.3-μm UIR bands in the CGS3 spectrum of this star.

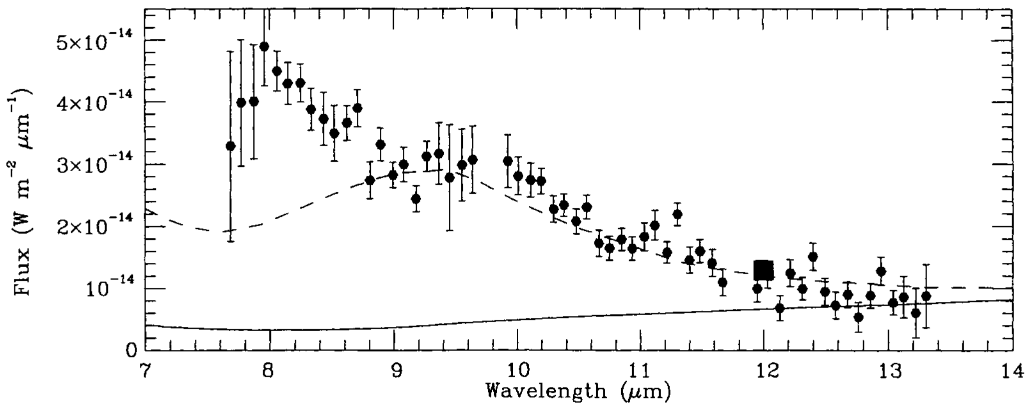

Figure 8. Detail of the SAO 183986 models in the mid-IR. Error bars: CGS3 spectrum; large square: *IRAS* point; solid line: model B21p8; dashed line: effect of adding small grains.

Table 6. Models for SAO 184124 (HD 144432).

Model	γ	β	R_{in} au	R_{out} au	M_{disc} $M_\odot$	a_{max} μm	F_{12}	F_{25}	F_{60}	F_{100}	$F_{0.8}$	$F_{1.1}$
								Jy				mJy
Observations							7.6	9.2	5.7	3.3	103	72
(± error)							0.5	0.6	0.6	0.3	34	12
M31	3	1	10.7	1100	9.6×10^{-6}	1000	1.6	9.9	5.7	2.9	36	13
M22	2	2	3.3	1100	1.7×10^{-6}	1000	3.8	9.9	5.9	2.6	60	26
M21	2	1	2.1	1100	2.7×10^{-5}	1000	3.5	7.7	5.7	3.5	230	110
M21p3	2	1.3	2.3	1100	9.6×10^{-6}	1000	4.1	8.9	5.6	2.9	121	55
M21p2	2	1.2	2.5	1100	1.4×10^{-5}	1000	3.3	8.0	5.6	3.1	152	70
M13	1	3	4.7	1100	2.7×10^{-6}	1000	2.1	8.2	5.7	2.7	90	42
M12	1	2	4.0	1100	7.0×10^{-6}	1000	2.0	9.4	5.7	3.0	114	57
M11p8	1	1.8	3.3	1100	9.5×10^{-6}	1000	2.6	7.9	5.7	3.0	124	62
B31	3	1	16.7	1100	1.2×10^{-6}	1000	2.7	8.2	5.6	2.7	31	11
B22	2	1	5.3	1100	3.0×10^{-6}	1000	2.4	7.9	5.7	2.7	67	29
B21	2	2	2.7	1100	3.3×10^{-5}	1000	3.4	7.7	5.8	3.5	215	100
B21p5	2	1.5	4.0	1100	8.0×10^{-6}	1000	2.9	8.1	5.6	2.9	96	43
B21p3	2	1.3	4.0	1100	1.5×10^{-5}	1000	2.5	7.4	5.6	3.1	130	60
B12	1	2	4.0	1100	8.4×10^{-6}	1000	2.8	8.4	5.7	2.8	103	51
B11	1	1	2.0	1100	1.1×10^{-4}	1000	3.6	7.3	5.5	3.6	360	190
B11p8	1	1.8	4.0	1100	1.3×10^{-5}	1000	2.5	7.8	5.6	2.9	121	61

6.5 SAO 184124 (HD 144432)

This A9/F0V star (Houk 1982) was first listed as a Vega-excess star by Walker & Wolstencroft (1988). Gregorio-Hetem et al. (1992) suggested that it is a Herbig Ae star, and Dunkin et al. (1997b) have illustrated its optical emission-line spectrum. It has the highest contrast silicate feature of any source in our sample (Paper I); this feature has also been detected by Walker & Butner (1995).

A grid of pure silicate models was run (models M31–M11p8: see Table 6), as well as a second grid using a mixture of silicate and AC grains, in a 3:1 ratio (models B31–B11p8). Model B21p3 gave good agreement with both JCMT points, and is presented in Fig. 9.

Using the small-grain technique to attempt to fit the near-IR excess of SAO 184124, it was found that both 5 and 3 Å radius grains of silicate or AC located 3.3 au from the star exhibited thermal spiking, but the resulting emission peaked at wavelengths that were too long to give a satisfactory fit to the observed near-IR excess. A good fit to the observed near-IR excess could be found for 5-Å silicate grains at 0.22 au, and for amorphous carbon grains of

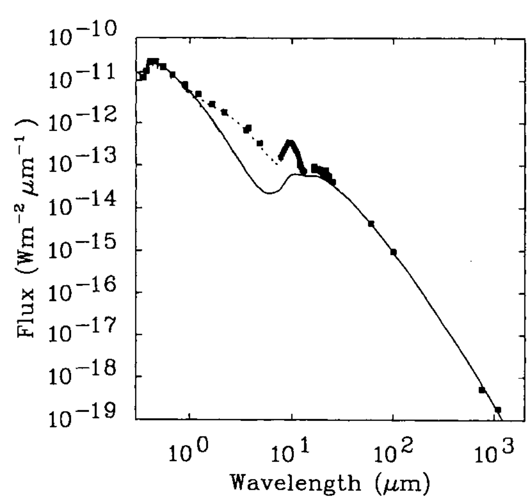

Figure 9. Results of modelling SAO 184124. Solid line: model B21p3; dotted line: effect of adding small silicate and AC grains in thermal equilibrium ($T \approx 1100$ K) to model B21p3.

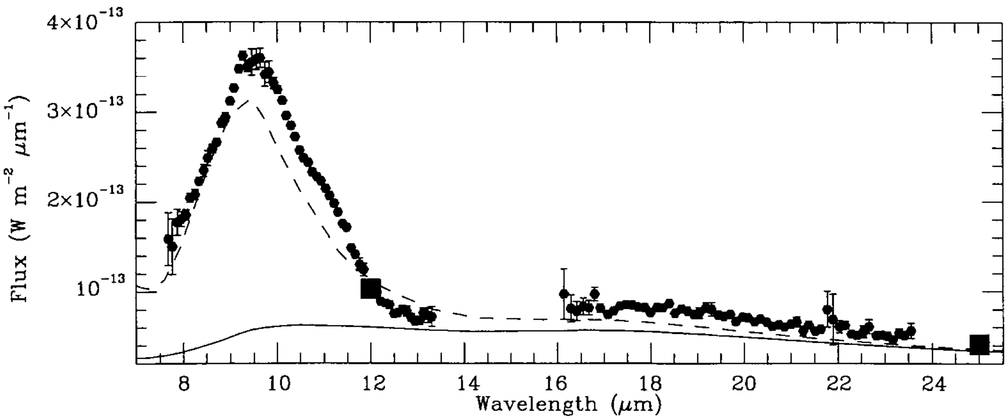

Figure 10. Detail of the SAO 184124 models in the mid-IR. Error bars: CGS3 spectrum; large squares: *IRAS* points; solid line: model B21p3; dashed line: effect of adding small grains (see text).

Table 7. Models for SAO 186777 (HD 169142).

Model	γ	β	R_{in} au	R_{out} au	M_{disc} $M_\odot$	a_{max} μm	F_{12}	F_{25} Jy	F_{60}	F_{100}	$F_{0.8}$ mJy	$F_{1.1}$
Observations							2.95	18.4	30	23.4	554	287
(± error)							0.17	1.1	3	2.0	34	13
B33	3	3	210	1450	1.3×10^{-5}	1000	1.01	16.3	33	20.0	221	78
B31	3	1	120	1450	1.9×10^{-5}	1000	1.58	17.0	30	19.7	266	95
B23	2	3	25	1450	3.6×10^{-5}	1000	1.99	18.3	29	18.7	547	236
B22	2	2	23	1450	9.0×10^{-5}	1000	1.85	17.4	30	21.1	810	358
B13	1	3	18	1450	8.5×10^{-5}	1000	1.63	19.1	30	18.6	753	374
B14	1	4	20	1450	7.0×10^{-5}	1000	1.46	18.8	30	18.5	708	350
B2p52	2.5	2	80	1450	6.7×10^{-5}	1000	1.86	18.1	31	22.1	635	253
B2p52a	2.5	2	80	1450	1.7×10^{-4}	10000	1.77	17.3	30	21.3	627	252
B2p51p5	2.5	1.5	60	1450	7.8×10^{-5}	1000	2.27	19.1	30	20.8	638	256

the same size at 0.47 au. The peak (near-equilibrium) temperatures of both grain species were approximately 1100 K. A mass of $6\times10^{-7}M_{\rm Earth}$ of silicate grains, or $1\times10^{-6}M_{\rm Earth}$ of AC grains, was needed.

Using only small silicate grains gave a 10-μm silicate feature with higher contrast than that observed in the CGS3 spectrum. Combining the two 'hot' small-grain models, with equal weightings, gave a reasonable fit to the CGS3 data. The effects of adding this combined model to disc model B21p3 are shown in Figs 9 and 10.

6.6 SAO 186777 (HD 169142)

SAO 186777 was first noted as a Vega-excess star by Walker & Wolstencroft (1988). It was classified as a B9V star by Houk (1982), and shows Hα in emission (Merrill & Burwell 1949). It has recently been reclassified as an A5e star on the basis of echelle spectra (Dunkin et al. 1997a).

SAO 186777 was the first Vega-excess star discovered to show the UIR bands in its mid-IR spectrum (Sylvester, Barlow & Skinner 1994). Since the 20-μm spectrum of this source shows weak silicate emission, models were run using a mixture of silicate and amorphous carbon grains, with the carbon grains making up 20 per cent of the total dust mass. The new spectral type of A5Ve from Dunkin et al. (1997a) was adopted.

Two models were run with a grain size parameter of $\gamma=3$ (models B33, B31: see Table 7). Both gave significantly too little flux at millimetre wavelengths. Of the γ=2 models, model B23 gave reasonable agreement with the JCMT data (Fig. 11), while model B22 gave mm-wave fluxes that were somewhat too high.

Essentially all of the model flux in the mid-IR is predicted to emerge from the inner few arcsec of the disc, so the difference between the CGS3 and *IRAS* fluxes does not appear to be due to a beam size effect. Scaling the CGS3 fluxes up by a factor of 1.3 gives good agreement between the *IRAS* and CGS3 fluxes at 12 μm, and between the model and the 20-μm spectrum (see Fig. 12).

Again, it was found that emission from 5 and 3 Å radius thermally spiking grains of silicate or AC peaked at longer wavelengths than the observed near-IR excess. Reducing the distance of the small grains from the star to 0.67 au for 5 Å radius grains of amorphous carbon gave good agreement with the observed near-IR excess. The grains were found to be close to thermal equilibrium, with a most probable temperature of 1150 K. A mass of $1.2\times10^{-6}M_{\rm Earth}$ of such grains was required. Adding this model to model B23 gave good agreement to all the photometry, but slightly too much flux at 12 μm in the 10-μm spectrum (Fig. 12). Most of the 10 μm region flux can be seen to be due to emission in the 7.7-, 8.6- and 11.3-μm bands.

6.7 SAO 206462 (HD 135344)

Coulson & Walther (1995) made extensive optical, IR and mm-wave observations of this star. They found that its spectral type is misclassified in the SAO catalogue: it shares the same HD number

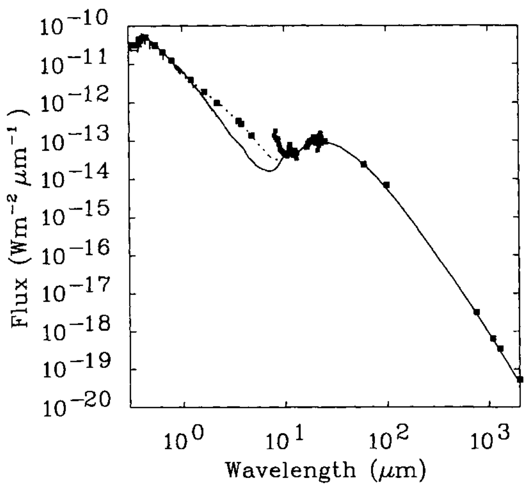

Figure 11. Results of modelling SAO 186777. Solid line: model B23; dotted line: effect of adding hot ($T \approx 1150$ K) grains in thermal equilibrium.

as SAO 206463, and the A2 classification appropriate for SAO 206463 is repeated for SAO 206462. The Michigan catalogue gives a combined spectral type of A0V. Coulson & Walther determined a spectral type for SAO 206462 of F8V. An F-type classification is consistent with the observations of Oudmaijer et al. (1992: F4Ve), Zuckerman et al. (1995: F6V) and Dunkin et al. (1997a: F4Ve).

Coulson & Walther (1995) modelled the IR excess emission of SAO 206462 with two blackbodies – one of temperature 1500 K, which fitted the near-IR excess, and one of temperature 95 K, which fitted the long-wavelength data.

A grid of grain blend models was run (models B22–B2p73: Table 8), along with two models using only AC grains (models C21–C11). No attempt was made to fit the *IRAS* 12-μm flux, since the 12-μm band contains strong UIR-band emission, which is not treated by the model. The spectral energy distribution of the best-fitting model (B2p73) is presented in Fig. 13, and the fit to the mid-IR region is shown in Fig. 14.

The small-grain code was used to try to fit the near-IR excess of SAO 206462. 5 and 3 Å radius grains of AC at 93 au from the star (the inner radius of model B2p73) displayed thermal spiking, but the resulting spectrum peaked at too long a wavelength.

The distance of the 5-Å grains from the star was decreased until a fit to the near-IR excess emission was obtained. A distance of 0.27 au gave good agreement. The grains were close to thermal equilibrium, with a peak temperature of 1060 K. The mass of 5 Å radius amorphous carbon grains required to match the near-IR flux was $3 \times 10^{-7} M_{\mathrm{Earth}}$, equivalent to the mass of a 100-km diameter asteroid. The effect of adding this amount of hot material is illustrated in Fig. 13, while their contribution to the mid-IR spectrum is shown in Fig. 14.

6.8 SAO 226057 (HD 139614)

A grid of models (see Table 9) was run for the A7Ve star SAO 226057, using only silicate dust for models M22–M1p51p5. The disc mass and outer radius were adjusted to fit the *IRAS* fluxes at 25 and 60 μm. Given that the long-wavelength tail of the strong near-IR excess may contribute to the 12-μm flux, the *IRAS* 12-μm point was treated as an upper limit to the flux from the equilibrium models. Model M21p3 gives a good fit to the data from 25 μm to 1 mm, and is presented in Fig. 15.

A further grid (models B22–B11p7) was produced, using a blend of 75 per cent silicate and 25 per cent AC grains. Similar results were obtained as for the pure silicate models.

Two models were run using only AC grains (models C11 and C0p50p5). Both gave significantly too little long-wavelength flux, even with rather low values of γ and β.

The near-IR excess of SAO 226057 was modelled using the small-grain technique. Grains of radius 5 Å located 67 au from the star (the inner radius of model M21p3) showed departures from thermal equilibrium, but the peak wavelength of the resulting emission spectrum was too long.

3 Å radius grains gave better results, although the fit to the near-IR observations was not perfect, with too much flux in the *M* band, and too little at *H*. A harder UV–optical radiation field than that predicted by the Kurucz model atmosphere would increase the probability of high-temperature excursions, and so cause the small-grain emission to peak at shorter wavelengths.

The narrow-band 10-μm photometry of van der Veen et al. (1989) of SAO 226057 does not suggest the presence of a strong silicate feature, so only amorphous carbon grains were considered in the small-grain modelling. The mass of thermally spiking small grains at 67 au required to reproduce the near-IR flux distribution

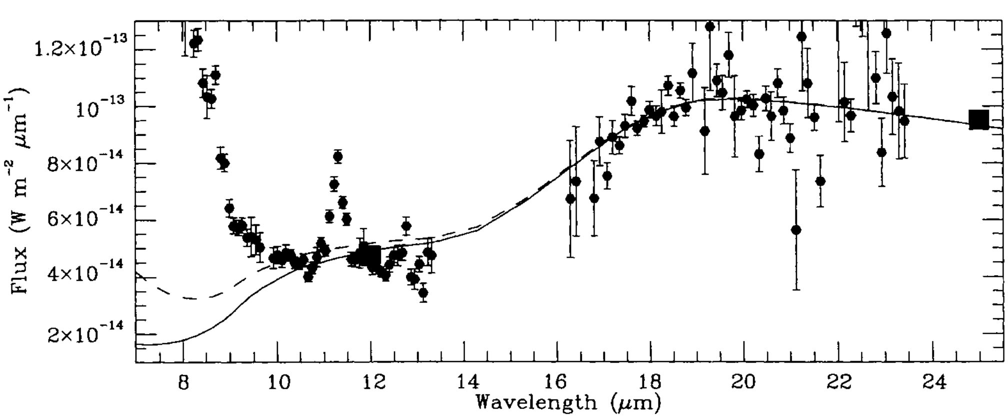

Figure 12. Detail of the SAO 186777 models in the mid-IR. Error bars: CGS3 spectrum scaled up by a factor of 1.3; large squares: *IRAS* points; solid line: model B23; dashed line: effect of adding small grains.

Table 8. Models for SAO 206462 (HD 135344).

Model	γ	β	R_{in} au	R_{out} au	M_{disc} $M_\odot$	a_{max} μm	F_{12} Jy	F_{25} Jy	F_{60} Jy	F_{100} Jy	$F_{0.8}$ mJy	$F_{1.1}$ mJy
Observations							1.59	6.7	25.6	25.7	570	209
(± error)							0.01	0.9	3.6	2.6	21	14
B22	2	2	23	840	1.2×10^{-4}	1000	0.33	6.5	25.5	26.2	>1 Jy	809
B32	3	2	120	840	1.1×10^{-5}	1000	0.19	6.2	25.3	21.7	389	140
B23	2	3	27	840	6.0×10^{-5}	1000	0.31	6.4	25.6	25.8	>1 Jy	617
B24	2	4	27	840	4.0×10^{-5}	1000	0.33	6.5	24.8	23.9	>1 Jy	493
B31	3	1	93	840	1.7×10^{-5}	1000	0.25	6.5	25.5	23.0	483	176
B2p51	2.5	1	53	840	1.3×10^{-5}	1000	0.34	6.3	26.2	27.4	>1 Jy	716
B2p52	2.5	2	67	840	6.4×10^{-5}	1000	0.32	6.5	26.2	25.0	>1 Jy	469
B2p53	2.5	3	73	840	4.1×10^{-5}	1000	0.32	6.6	25.9	23.8	922	372
B2p54	2.5	4	73	840	3.0×10^{-5}	1000	0.32	7.1	25.9	22.8	788	314
B2p72	2.7	2	87	840	3.0×10^{-5}	1000	0.28	6.5	25.6	23.1	676	261
B2p73	2.7	3	93	840	2.0×10^{-5}	1000	0.26	6.7	25.3	21.6	543	207
C22	2	2	37	840	2.0×10^{-4}	1000	0.39	6.5	25.3	17.8	186	64
C21	2	1	29	840	6.0×10^{-4}	1000	0.43	6.5	25.7	21.6	373	135
C11	1	1	23	840	2.4×10^{-3}	1000	0.15	6.4	25.6	20.7	344	124

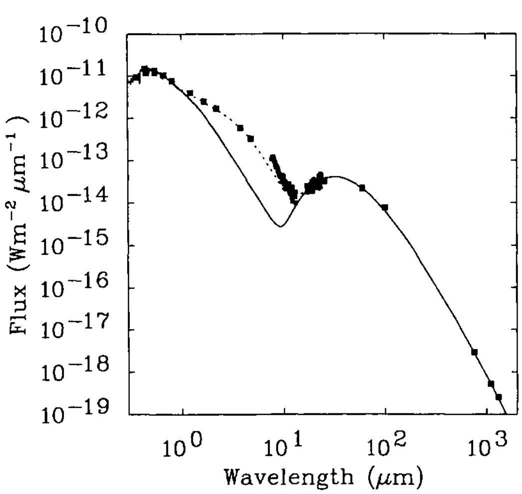

Figure 13. Results of modelling SAO 206462. Solid line: model B2p73; dotted line: effect of adding hot grains in thermal equilibrium ($T\approx1000$ K) to model B2p73.

was 6×10^{23} g ($10^{-4}M_{\rm Earth}$). The effects of adding thermally spiking grains to model M21p3 are shown in Fig. 15.

7 DISCUSSION

Table 10 lists the parameters of the best-fitting models of the set of eight stars modelled in this paper, as well as those from Paper II. The stars are ordered by spectral type. The power-law indices γ and β do not appear to correlate with spectral type. The derived values of the grain-size power-law index γ lie in the range 2–3. An MRN-like distribution (Mathis, Rumpl & Nordsieck 1977) would have γ=2.5 (Paper II), so it appears that the grain size distribution in Vega-like discs may resemble the MRN distribution, extended to larger grain sizes. All the models used minimum and maximum grain radii of 50 Å and 1000 μm respectively. For $\gamma < 3$, the majority of the grain mass resides in the largest grains in the distribution. When the maximum grain size is unknown, therefore, the total dust mass is poorly constrained. There is some tendency for the later type stars to have lower disc masses. Also, of the six G- or K-type stars, only one has a near-IR excess, while of the six stars of type A5 or earlier,

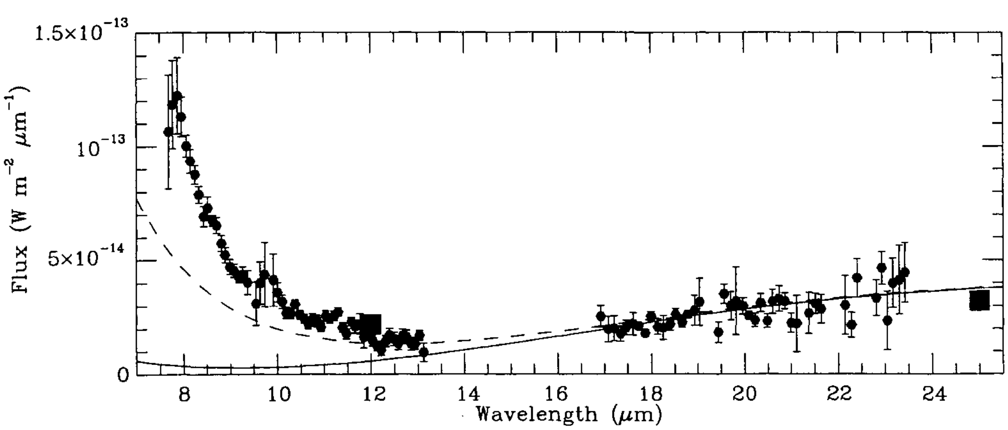

Figure 14. Detail of the SAO 206462 models in the mid-IR. Error bars: CGS3 spectrum; large squares: *IRAS* points; solid line: model B2p73; dashed line: effect of adding small grains.

Table 9. Models for SAO 226057 (HD 139614).

Model	γ	β	R_{in} au	R_{out} au	M_{disc} $M_\odot$	a_{max} µm	F_{12} Jy	F_{25} Jy	F_{60} Jy	F_{100} Jy	$F_{0.8}$ mJy	$F_{1.1}$ mJy
Observations							4.1	18.1	19.3	13.9	608	272
(± error)							0.2	2.5	2.7	2.0	27	13
M22	2	2	9.3	1500	2.3×10^{-5}	1000	3.1	18.3	19.3	10.7	317	138
M21	2	1	5.3	1500	2.4×10^{-4}	1000	4.3	18.3	19.3	13.2	>1Jy	481
M21p3	2	1.3	6.7	1500	1.1×10^{-4}	1000	3.6	18.1	19.3	12.1	623	286
M21p5	2	1.5	7.3	1500	6.4×10^{-5}	1000	3.4	18.2	19.2	11.5	475	214
M31	3	1	32.0	1500	1.3×10^{-5}	1000	1.0	18.0	19.3	11.4	165	59
M30p5	3	0.5	16.0	1500	2.5×10^{-5}	1000	2.2	18.1	19.3	13.9	266	97
M2p51	2.5	1	16.7	1500	7.5×10^{-5}	1000	2.1	18.0	19.2	12.8	504	209
M12	1	2	7.3	1500	6.7×10^{-5}	1000	3.0	18.4	19.4	11.2	488	254
M11p7	1	1.7	6.5	1500	1.2×10^{-4}	1000	3.3	18.2	19.2	11.5	595	303
M1p51p5	1.5	1.5	5.9	1500	1.3×10^{-4}	1000	3.6	18.2	19.3	11.9	661	325
B22	2	2	11.3	1500	3.5×10^{-5}	1000	3.2	18.1	19.3	10.8	324	141
B21	2	1	6.6	1500	3.0×10^{-4}	1000	4.4	18.2	19.3	13.1	939	442
B21p3	2	1.3	8.7	1500	1.4×10^{-4}	1000	3.9	18.2	19.3	12.0	596	273
B31	3	1	47.0	1500	1.1×10^{-5}	1000	3.5	18.1	19.2	10.9	139	50
B12	1	2	8.7	1500	9.7×10^{-5}	1000	3.0	18.2	19.3	11.2	492	248
B11p7	1	1.7	8.0	1500	1.7×10^{-4}	1000	3.3	18.2	19.3	11.6	603	308
C11	1	1	13.3	1500	2.4×10^{-3}	1000	2.6	18.1	19.3	10.6	127	45
C0p50p5	0.5	0.5	4.5	1500	7.6×10^{-3}	1000	6.1	18.1	19.3	14.4	274	99

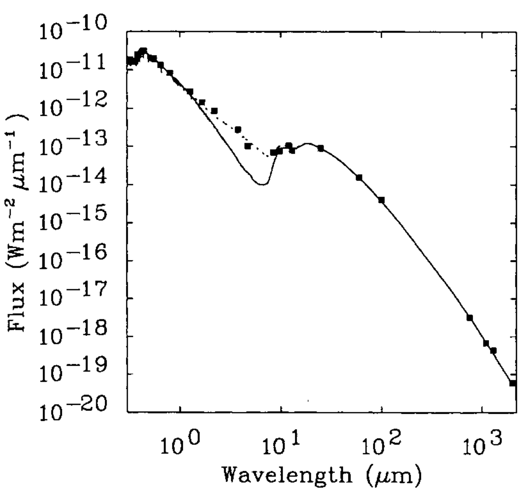

Figure 15. Results of modelling SAO 226057. Solid line: model M21p3; dotted line: effect of adding small thermally spiking AC grains to model M21p3.

three have near-IR excesses. However, our sample size is too small to claim a strong correlation.

As shown in the preceding figures and tables, the combined models can give very good fits to the observational data. The equilibrium models are rather well constrained. This agrees with the results of Paper II: the current stars all have rather large fractional excess luminosities, and the SED of the excess emission is well defined by the observations over a large wavelength range. However, separating the models for the near-IR excess from the equilibrium models leads to some uncertainty in the interpretation of the CGS3 spectra, as the small grains can be responsible for a noticeable fraction of the 10-µm silicate emission. The CGS3 spectra are thus less useful for constraining the grain size distribution parameter γ than might be hoped. On the other hand, the stars in the current paper have good mm-wave detections, allowing us to put constraints on γ using the mm-wave emission from large grains (see Paper II for discussion of the effects of the modelling parameters). Imaging observations in the IR or submm would help to constrain the models, by providing an independent determination of the disc density distribution parameter β.

The thermal equilibrium disc models alone do not always provide sufficient contrast in the 10-µm silicate feature; this is because the grain size distributions must contain an amount of large grains (which show no silicate feature) that is sufficient to provide the observed mm-wave emission. A size distribution that was not described by a single power law could, in principle, give the right proportions of small and large grains to fit both the long-wavelength emission and the silicate features, without requiring any contribution to the feature contrast from the very small grains. However, such a distribution would mean introducing more free parameters into the distribution.

Thermally spiking small grains do not generally give good fits to the observed near-IR excess SEDs. Reasonable fits were obtained with thermally spiking 3 Å radius grains for SAO 77144 and 131926, which are both classified as early A-type stars, and are the hottest of our stars to show near-IR excesses. For the other stars, the resulting SEDs from spiking grains peaked at wavelengths that were too long. Hotter stars will emit more UV photons, so it is it to be expected that they will more easily excite small grains to high temperatures. Emission from thermally spiking grains could be responsible for the near-IR excesses of the other stars if there is, for instance, excess UV emission from the stars, or the small grains have a greater UV absorption cross-section than was adopted for the present modelling. However, given the large $L_{IR}/L_\star$ values of the current sample (0.14–0.64), it seems highly unlikely that any of the stars could have sufficiently large UV excesses to power the observed near-IR luminosities.

Léger & d'Hendecourt (1987) have shown that small graphitic clusters only absorb photons with energy greater than

Table 10. Best-fitting model parameters. Results from Paper II (in parentheses) are included for comparison.

SAO	HD	Spectral Type	γ	β	R_{in} (au)	$R_{in,proj}$ (arcsec)	M_{disc} ($M_{\odot}$)
131926	34282	A0	2.7	2	635	1.2	8×10^{-4}
(140789	141569	A0Ve	3	2	670	3.5	7×10^{-6})
(147886	9672	A1V	:	:	$\gtrsim$150	$\gtrsim$2	$\gtrsim10^{-7}$)
77144	35187	A2/3 IV/Ve	2.5	0.7	8.7	0.06	4×10^{-5}
186777	169142	A5Ve	2	3	24.7	0.1	4×10^{-5}
(91022	218396	A5V	:	:	$\gtrsim$5	$\gtrsim$0.1	$\gtrsim10^{-8}$)
226057	139614	A7Ve	2	1.3	7.4	0.05	6×10^{-5}
183956	142666	A8Ve	2	0.9	2.7	0.02	5×10^{-5}
184124	144432	A9/F0Ve	2	1.3	4.0	0.03	2×10^{-5}
206462	135344	F8Ve	2.7	3	93.6	1.1	2×10^{-5}
(112630	34700	G0	3	3	46	0.8	8×10^{-7})
183986	143006	G5Ve	2	1.8	6.5	0.08	2×10^{-5}
(93601	23680	G5	:	:	$\gtrsim$40	$\gtrsim$2	$\gtrsim10^{-7}$)
(158350	123160	G5	3	3	190	12	2×10^{-7})
(111388	23362	K2	:	:	$\gtrsim$4	$\gtrsim$0.6	$\gtrsim10^{-9}$)
(179815	98800	K5Ve	2.2	1.6	1.1	0.05	4×10^{-7})

An 'e' in the spectral type column indicates the presence of Hα emission (Dunkin et al., in preparation).

some threshold value due to their possessing only discrete electronic states. For a 50-atom cluster, the threshold is a few eV, corresponding to wavelengths of a few hundred nm. This makes the effective radiation field with which the cluster can interact 'harder' than the stellar radiation field. If the thermally spiking grains around Vega-excess stars were small enough for this effect to be important, they would, on average, reach higher temperatures after a spiking event, and the resulting near-IR flux would peak at shorter wavelengths.

Natta et al. (1993a) constructed models of the circumstellar environments of Herbig AeBe (HAeBe) stars using the technique of Siebenmorgen et al. (1992), which incorporates thermally spiking small grains. The minimum grain size was 5 Å, and the stellar temperatures were in the range 10 000–20 000 K (hotter than most of our stars). Their conclusions are similar to those we reached for our models. They found that thermally spiking grains can contribute a significant fraction of the mid-IR luminosity of AeBe stars, but that the near-IR colours of the small-grain emission did not give satisfactory agreement with observations of HAeBe stars. The overall range of model near-IR colours obtained by Natta et al. does overlap our observed colours of Vega-like stars (Paper I), but the observed points lie outside the detailed loci of the models on colour–colour diagrams.

The near-equilibrium temperatures derived by modelling small grains close to the stars lie in the range 1000–1500 K, which are similar to typical dust condensation/evaporation temperatures (e.g. Gilman 1969). If the grains are not thermally spiking, it is not clear that they could survive indefinitely at these temperatures. The near-IR emission may therefore arise from a population of grains that is falling in towards the star (due to e.g. Poynting–Robertson drag), and which are being evaporated as they approach the star. Note that the hot grains in thermal equilibrium need not be very small; large grains close to the star could also provide near-IR emission. Another way to provide a supply of hot grains is by having comet-like bodies passing close to the star and releasing material, as has been postulated to explain the variable absorption lines in the spectrum of β Pic (e.g. Beust et al. 1990).

The large fractional excess luminosities of these stars (Table 1) imply the discs cannot be physically thin and emitting only reprocessed starlight. To intercept enough starlight, reprocessing 'discs' must subtend a large solid angle, i.e. they must be substantially flared, or alternatively some of the dust may reside in a spherical envelope. Many HAeBe stars are believed to possess large spherical envelopes as well as discs. It is of interest to consider whether the double-peaked Vega-excess SEDs could be due to a hot disc and a cooler, more distant envelope. Because our models are optically thin, the SED of a spherical envelope is identical to that of a disc with the same parameters (γ, β, etc.). We can therefore immediately compare the derived properties of the discs with those of HAeBe envelopes. Natta et al. (1993b) derived envelope inner radii in the range $\sim$1400–2×10^4 au for a sample of five HAeBe stars; the envelope masses were all greater than $\sim$10 $M_{\odot}$. In contrast, the disc masses in Table 10 are all less than 10^{-3} $M_{\odot}$. The inner radii we derive for Vega-like systems are much smaller than those found by Natta et al. for the HAeBe envelopes: only SAO 131926 has an inner radius within a factor of 10 of the smallest HAeBe envelope inner radius. Hence if the dust around these 'extreme' Vega-excess stars is distributed in spherical envelopes, they are very different from HAeBe envelopes.

Another possible explanation for the large fractional excess luminosities is intrinsic disc luminosity. This can arise from the conversion of gravitational potential energy due to material accreting through the disc. If we assume that the discs intercept and re-radiate the 'flat disc' maximum of $0.25L_{\star}$, then the remaining excess luminosity L_i is intrinsic to the disc, and can be assumed to be due to accretion. We can then derive the accretion luminosity and the mass accretion rate $\dot{M}_{acc}$, using the relation $\dot{M}_{acc}=R_{\star}L_i/GM_{\star}$ (see Natta et al. 1993b for details). The values of $\dot{M}_{acc}$ calculated for our stars are presented in Table 11. These values seem plausible: the largest value (for SAO 131926) is comparable to the smallest values derived by Hillenbrand et al. (1992) for a sample of 23 HAeBe stars, while the others are all smaller than any derived by Hillenbrand et al. They are also considerably smaller than the typical protostellar accretion rate of 10^{-5} $M_{\odot}$ yr^{-1} adopted by Palla & Stahler (1993).

Table 9. Models for SAO 226057 (HD 139614).

Model	γ	β	R_{in} au	R_{out} au	M_{disc} $M_\odot$	a_{max} µm	F_{12}	F_{25} Jy	F_{60}	F_{100}	$F_{0.8}$	$F_{1.1}$ mJy
Observations							4.1	18.1	19.3	13.9	608	272
(± error)							0.2	2.5	2.7	2.0	27	13
M22	2	2	9.3	1500	2.3×10^{-5}	1000	3.1	18.3	19.3	10.7	317	138
M21	2	1	5.3	1500	2.4×10^{-4}	1000	4.3	18.3	19.3	13.2	>1Jy	481
M21p3	2	1.3	6.7	1500	1.1×10^{-4}	1000	3.6	18.1	19.3	12.1	623	286
M21p5	2	1.5	7.3	1500	6.4×10^{-5}	1000	3.4	18.2	19.2	11.5	475	214
M31	3	1	32.0	1500	1.3×10^{-5}	1000	1.0	18.0	19.3	11.4	165	59
M30p5	3	0.5	16.0	1500	2.5×10^{-5}	1000	2.2	18.1	19.3	13.9	266	97
M2p51	2.5	1	16.7	1500	7.5×10^{-5}	1000	2.1	18.0	19.2	12.8	504	209
M12	1	2	7.3	1500	6.7×10^{-5}	1000	3.0	18.4	19.4	11.2	488	254
M11p7	1	1.7	6.5	1500	1.2×10^{-4}	1000	3.3	18.2	19.2	11.5	595	303
M1p51p5	1.5	1.5	5.9	1500	1.3×10^{-4}	1000	3.6	18.2	19.3	11.9	661	325
B22	2	2	11.3	1500	3.5×10^{-5}	1000	3.2	18.1	19.3	10.8	324	141
B21	2	1	6.6	1500	3.0×10^{-4}	1000	4.4	18.2	19.3	13.1	939	442
B21p3	2	1.3	8.7	1500	1.4×10^{-4}	1000	3.9	18.2	19.3	12.0	596	273
B31	3	1	47.0	1500	1.1×10^{-5}	1000	3.5	18.1	19.2	10.9	139	50
B12	1	2	8.7	1500	9.7×10^{-5}	1000	3.0	18.2	19.3	11.2	492	248
B11p7	1	1.7	8.0	1500	1.7×10^{-4}	1000	3.3	18.2	19.3	11.6	603	308
C11	1	1	13.3	1500	2.4×10^{-3}	1000	2.6	18.1	19.3	10.6	127	45
C0p50p5	0.5	0.5	4.5	1500	7.6×10^{-3}	1000	6.1	18.1	19.3	14.4	274	99

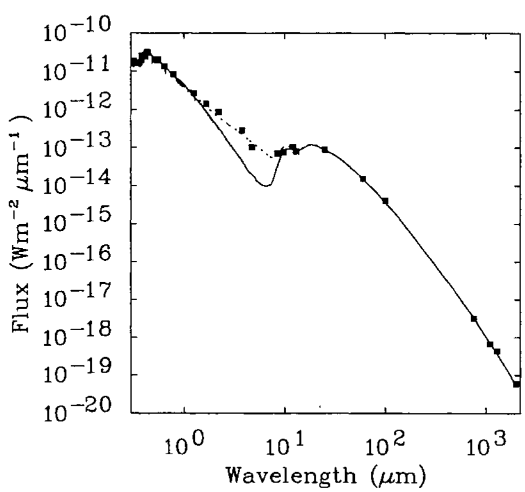

Figure 15. Results of modelling SAO 226057. Solid line: model M21p3; dotted line: effect of adding small thermally spiking AC grains to model M21p3.

three have near-IR excesses. However, our sample size is too small to claim a strong correlation.

As shown in the preceding figures and tables, the combined models can give very good fits to the observational data. The equilibrium models are rather well constrained. This agrees with the results of Paper II: the current stars all have rather large fractional excess luminosities, and the SED of the excess emission is well defined by the observations over a large wavelength range. However, separating the models for the near-IR excess from the equilibrium models leads to some uncertainty in the interpretation of the CGS3 spectra, as the small grains can be responsible for a noticeable fraction of the 10-µm silicate emission. The CGS3 spectra are thus less useful for constraining the grain size distribution parameter γ than might be hoped. On the other hand, the stars in the current paper have good mm-wave detections, allowing us to put constraints on γ using the mm-wave emission from large grains (see Paper II for discussion of the effects of the modelling parameters). Imaging observations in the IR or submm would help to constrain the models, by providing an independent determination of the disc density distribution parameter β.

The thermal equilibrium disc models alone do not always provide sufficient contrast in the 10-µm silicate feature; this is because the grain size distributions must contain an amount of large grains (which show no silicate feature) that is sufficient to provide the observed mm-wave emission. A size distribution that was not described by a single power law could, in principle, give the right proportions of small and large grains to fit both the long-wavelength emission and the silicate features, without requiring any contribution to the feature contrast from the very small grains. However, such a distribution would mean introducing more free parameters into the distribution.

Thermally spiking small grains do not generally give good fits to the observed near-IR excess SEDs. Reasonable fits were obtained with thermally spiking 3 Å radius grains for SAO 77144 and 131926, which are both classified as early A-type stars, and are the hottest of our stars to show near-IR excesses. For the other stars, the resulting SEDs from spiking grains peaked at wavelengths that were too long. Hotter stars will emit more UV photons, so it is it to be expected that they will more easily excite small grains to high temperatures. Emission from thermally spiking grains could be responsible for the near-IR excesses of the other stars if there is, for instance, excess UV emission from the stars, or the small grains have a greater UV absorption cross-section than was adopted for the present modelling. However, given the large $L_{IR}/L_\star$ values of the current sample (0.14–0.64), it seems highly unlikely that any of the stars could have sufficiently large UV excesses to power the observed near-IR luminosities.

Léger & d'Hendecourt (1987) have shown that small graphitic clusters only absorb photons with energy greater than unreddened, the model $E(B-V)$ is 0.24, while τ_V is 0.62; the dust therefore cannot be distributed in a shell and have the properties adopted for the models that fit the SED. To obtain a shell that gives sufficient $L_{\rm IR}/L_\star$ without appreciable reddening would require dust with a high R_V (ratio of total to selective extinction). This implies a much shallower grain size distribution than used by the best-fitting model. Such a distribution would have emission properties inconsistent with the observations, giving much larger far-IR and mm-wave fluxes than are observed (Table 8). A disc therefore remains the most plausible distribution for the matter around this star.

ACKNOWLEDGMENTS

We thank the UKIRT staff, particularly Tom Geballe, John Davies and Dolores Walther, for obtaining the CGS4 spectrum in Service time. The United Kingdom Infrared Telescope is operated by the Joint Astronomy Centre on behalf of the UK Particle Physics and Astronomy Research Council. This work was supported in part (CJS) under the auspices of the US Dept of Energy under Contract No. W-7405-ENG-48 to the Lawrence Livermore National Laboratory at the Institute of Geophysics & Planetary Physics. We thank the Starlink project for the provision of computing facilities.

NOTE ADDED IN PROOF

Hipparcos parallaxes have recently been published (ESA 1997) for three of the stars in this paper: SAO 77144, 131926 and 184124 have parallaxes of 6.7 ± 2.5, 6.1 ± 1.6 and 4.0 ± 1.5 milliarcsec respectively, giving distances of 150 ± 50, 160 ± 40 and 250 ± 90 pc.

Comparing these with the adopted distances in Table 1, we find that SAO 77144 is slightly closer than the adopted distance, while SAO 184124 is at least twice as distant as our estimate, which suggests that it could lie above the main sequence. SAO 131926, on the other hand, lies much closer than the estimated 547 pc. This suggests that there could be a considerable amount of dust extinction in the line of sight, which could be due to an edge-on disc, as postulated by Bogaert & Waelkens (1991).

REFERENCES

Aumann H. H., 1985, PASP, 97, 885
Aumann H. H. et al., 1984, ApJ, 278, L23
Backman D. E., Paresce F., 1993, in Levy E. H., Lunine J. I., eds, Protostars & Planets III. Univ. of Arizona, Tucson, p. 1253
Beust H., Lagrange-Henri A. M., Vidal-Madjar A., Ferlet R., 1990, A&A, 236, 202
Bogaert E., Waelkens C., 1991, in Jaschek C., Andrillat Y., eds, The Infrared Spectral Region of Stars. Cambridge Univ. Press, Cambridge, p. 345
Böhm T., Catala C., 1995, A&A, 301, 155
Borkowski K. J., Harrington J. P., Blair W. P., Bregman J. D., 1994, ApJ, 435, 722
Boss A. P., Yorke H. W., 1996, ApJ, 469, 366
Coulson I. M., Walther D. M., 1995, MNRAS, 274, 977
de Muizon M., d'Hendecourt L. B., Geballe T. R., 1987, in Léger A., d'Hendecourt L. B., Boccara N., eds, NATO ASI Series C, 191, Polycyclic Aromatic Hydrocarbons and Astrophysics. Reidel, Dordrecht, p. 287
Dunkin S. K., Barlow M. J., Ryan S. G., 1997a, MNRAS, 286, 604
Dunkin S. K., Barlow M. J., Ryan S. G., 1997b, MNRAS, 290, 165
Ferlet R., Vidal-Madjar A., eds, 1994, Circumstellar Dust Disks and Planet Formation. Editions Frontières, Gif-sur-Yvette
Gilman R. C., 1969, ApJ, 155, L185
Greenberg J. M., 1968, in Middlehurst B. M., Aller L. H., eds, Nebulae & Interstellar Matter. Univ. of Chicago Press, Chicago, p. 221
Gregorio-Hetem J., Lepine J. R. D., Quast G. R., Torres C. A. O., de la Reza R., 1992, AJ, 103, 549
Grinin V. P., Kiselev N. N., Minikulov N. Kh., Chernova G. P., Voshchinnikov N. V., 1991, Ap&SS, 186, 283
Guhathakurta P., Draine B. T., 1989, ApJ, 345, 230 (GD89)
Hartmann L., Kenyon S. J., Calvet N., 1993, ApJ, 407, 219
Hillenbrand L. A., Strom S. E., Vrba F. J., Keene J., 1992, ApJ, 397, 613
Houk N., 1978, Michigan Catalogue of Two-Dimensional Spectral Types for the HD Stars Vol. 2. Univ. of Michigan, Ann Arbor
Houk N., 1982, Michigan Catalogue of Two-Dimensional Spectral Types for the HD Stars Vol. 3. Univ. of Michigan, Ann Arbor
Kurucz R. L., 1991, in Davis Philip A.G., Upgren A. R., Janes K. A., eds, Precision Photometry: Astrophysics of the Galaxy. L. Davis Press, Schenectady, p. 27
Léger A., d'Hendecourt L. B., 1987, in Léger A., d'Hendecourt L. B., Boccara N., eds, NATO ASI Series C, 191, Polycyclic Aromatic Hydrocarbons and Astrophysics. Reidel, Dordrecht, p. 223
Mathis J. S., Rumpl W., Nordsieck K. H., 1977, ApJ, 217, 425 (MRN)
Merrill P. W., Burwell C. G., 1949, ApJ, 110, 387
Miroshnichenko A. S., Bergner Yu. K., Kuratov K. S., Mukanov D. B., Sheikina T. A., 1996, Astron. Rep., 40, 509
Miroshnichenko A., Ivezić Ž., Elitzur M., 1997, ApJ, 475, L41
Natta A., Prusti T., Krügel E., 1993a, A&A, 275, 527
Natta A., Palla F., Butner H. M., Evans N. J., Harvey P. M., 1993b, ApJ, 406, 674
Oudmaijer R. D., van der Veen W. E. C. J., Trams N. R., Waelkens C., Engelsman E., 1992, A&AS, 96, 625
Palla F., Stahler S. W., 1993, ApJ, 418, 414
Schmidt-Kaler Th., 1982, in Schaifers K., Voigt H. H., eds, Landolt-Börnstein, Numerical Data and Functional Relationships in Science and Technology, Group VI, Astronomy, Astrophysics and Space Research, Vol. 2b. Springer-Verlag, Berlin, p. 14
Sellgren K., Werner M. W., Dinerstein H. L., 1983, ApJ, 271, L13
Siebenmorgen R., Krügel E., Mathis J. S., 1992, A&A, 266, 501
Skinner C. J., Barlow M. J., Justtanont K., 1992, MNRAS, 255, 31P
Skinner C. J., Sylvester R. J., Graham J. R., Barlow M. J., Meixner M., Keto E., Arens J. F., Jernigan J. G., 1995, ApJ, 444, 861
Sylvester R. J., Skinner C. J., 1996, MNRAS, 283, 457 (Paper II)
Sylvester R. J., Barlow M. J., Skinner C. J., 1994, Ap&SS, 212, 261
Sylvester R. J., Barlow M. J., Skinner C. J., Mannings V., 1996, MNRAS, 279, 915 (Paper I)
Turon C. et al., 1992, The *Hipparcos* Input Catalogue, ESA SP-1136
van der Veen W. E. C. J., Habing H. J., Geballe T. R., 1989, A&A, 226, 108
van der Veen W. E. C. J., Waters L. B. F. M., Trams N. R., Matthews H. E., 1994, A&A, 285, 551
Voit G. M., 1991, ApJ, 379, 122
Waelkens C., Bogaert E., Waters L. B. F. M., 1994, in The P. S., Perez M. R., van den Heuvel E. P. J., eds, ASP Conf. Ser. 62, The Nature and Evolutionary Status of Herbig Ae/Be Systems. Astron. Soc. Pac., San Francisco, p. 405
Walker H. J., Butner H. M., 1995, Ap&SS, 224, 389
Walker H. J., Wolstencroft R. D., 1988, PASP, 100, 1509
Zuckerman B., Forveille T., Kastner J. H., 1995, Nat, 373, 494

This paper has been typeset from a TEX/LATEX file prepared by the author.